

# Sensitive Probing of Exoplanetary Oxygen via Mid Infrared Collisional Absorption

Thomas J. Fauchez<sup>1,2,3</sup>, Geronimo L. Villanueva<sup>1,3</sup>, Edward W. Schwieterman<sup>4,5,6,7,8</sup>, Martin Turbet<sup>9</sup>, Giada Arney<sup>1,3,7</sup>, Daria Pidhorodetska<sup>1,10</sup>, Ravi K. Kopparapu<sup>1,3,7</sup>, Avi Mandell<sup>1,3</sup>, and Shawn D. Domagal-Goldman<sup>1,3,7</sup>

<sup>1</sup>NASA Goddard Space Flight Center, Greenbelt, Maryland, USA

<sup>2</sup>Goddard Earth Sciences Technology and Research (GESTAR), Universities Space Research Association, Columbia, Maryland, USA

<sup>3</sup>GSFC Sellers Exoplanet Environments Collaboration

<sup>4</sup>Department of Earth and Planetary Sciences, University of California, Riverside, California, USA

<sup>5</sup>NASA Postdoctoral Program, Universities Space Research Association, Columbia, Maryland, USA

<sup>6</sup>NASA Astrobiology Institute, Alternative Earths Team, Riverside, CA, USA

<sup>7</sup>Nexus for Exoplanet System Science (NExSS) Virtual Planetary Laboratory, Seattle, WA, USA

<sup>8</sup>Blue Marble Space Institute of Science, Seattle, Washington, USA

<sup>9</sup>Observatoire Astronomique de l'Université de Genève, Université de Genève, Chemin des Maillettes 51, 1290 Versoix, Switzerland.

<sup>10</sup>University of Maryland Baltimore County/CRESST II, 1000 Hilltop Cir. Baltimore, MD 21250, USA

Accepted in Nature Astronomy on 10/01/2019

Published in Nature astronomy on 06/01/2020

## Abstract

The collision-induced fundamental vibration-rotation band at  $6.4 \mu\text{m}$  is the most significant absorption feature from  $\text{O}_2$  in the infrared (Timofeyev & Tonkov, 1978; Rinsland et al., 1982, 1989), yet it has not been previously incorporated into exoplanet spectral analyses for several reasons. Either CIAs were not included or incomplete/obsolete CIA databases were used. Also, the current version of HITRAN does not include CIAs at  $6.4 \mu\text{m}$  with other collision partners ( $\text{O}_2\text{-X}$ ). We include  $\text{O}_2\text{-X}$  CIA features in our transmission spectroscopy simulations by parameterizing the  $6.4 \mu\text{m}$   $\text{O}_2\text{-N}_2$  CIA based on Rinsland et al. (1989) and the  $\text{O}_2\text{-CO}_2$  CIA based on Baranov et al. (2004). Here we report that the  $\text{O}_2\text{-X}$  CIA may be the most detectable  $\text{O}_2$  feature for transit observations. For a potential TRAPPIST-1e analogue system within 5 pc of the Sun, it could be the only  $\text{O}_2$  detectable signature with JWST (using MIRI LRS) for a modern Earth-like cloudy atmosphere with biological quantities of  $\text{O}_2$ . Also, we show that the  $6.4 \mu\text{m}$   $\text{O}_2\text{-X}$  CIA would be prominent for  $\text{O}_2$ -rich desiccated atmospheres (Luger & Barnes, 2015) and could be detectable with JWST in just a few transits. For systems beyond 5 pc, this feature could therefore be a powerful discriminator of uninhabited planets with non-biological "false positive"  $\text{O}_2$  in their atmospheres - as they would only be detectable at those higher  $\text{O}_2$  pressures.

## Main

We study the strength of the  $\text{O}_2\text{-X}$  CIA spectral signatures in exoplanets by computing synthetic spectra for various Earth-like atmospheres with the Planetary Spectrum Generator (PSG Villanueva et al. (2018)). The atmospheres are created with the LMD-G (Wordsworth et al., 2011) general circulation model (GCM) coupled with the Atmos (Arney et al., 2016) photochemical model (see Methods for details). We focus in particular on planets around M dwarfs such as TRAPPIST-1e. In fact, For modern Earth atmospheric conditions, the  $6.4 \mu\text{m}$  region is overlapped by a wide  $\text{H}_2\text{O}$  absorption band. However, for a modern Earth-like

atmosphere on a tidally locked planet in the HZ of an M dwarf, the terminator region is predicted to be fairly dry (see Supplementary Figure 2). Also, water is mostly confined in a small portion of the atmosphere near the surface and which is under the refraction limit and hidden by clouds (as on Earth, where the troposphere is wet and the stratosphere is dry). Near TOA, H<sub>2</sub>O is highly photodissociated (Supplementary Figure 2). The H<sub>2</sub>O signature in the transmission spectra of a habitable planet is therefore expected to be very weak (Lincowski et al., 2018; Lustig-Yaeger et al., 2019). While some trace gases such as NO<sub>2</sub> and N<sub>2</sub>O also produce opacity in this spectral region, their concentrations are predicted to be orders of magnitude lower than those that would generate confounding impacts on the simulated spectra.

The TRAPPIST-1 system (Gillon et al., 2017), consisting of seven Earth-sized planets orbiting an ultra-cool dwarf star, will be a favorite target for atmospheric characterization with JWST due to its relatively close proximity to the Earth and the depth and frequency of its planetary transits. Therefore, we use TRAPPIST-1e as a case study for our simulated spectra. We employed the LMD-G (Wordsworth et al., 2011) general circulation model (GCM) and the Atmos photochemical model (Arney et al., 2016) to simulate TRAPPIST-1e with boundary conditions similar to modern Earth (Lincowski et al., 2018).

Figure 1 shows TRAPPIST-1e transmission spectra from 0.6 to 10  $\mu\text{m}$  for various Earth-like atmospheres simulated with the Planetary Spectrum Generator (PSG, Villanueva et al. (2018)). The top panel shows the impact of cloud coverage on spectral features: clouds diminish the strength of all absorption features, but impact the strength of the O<sub>2</sub>-X feature much less strongly than they impact shorter wavelength O<sub>2</sub> features like the O<sub>2</sub> A-band or the 1.06 and 1.27  $\mu\text{m}$  O<sub>2</sub> CIA used in Misra et al. (2014) (who considered only clear-sky atmospheres). This is because water cloud opacity is stronger at short wavelengths. The middle panel compares the strength of the O<sub>2</sub>-X CIA band to the overlapping H<sub>2</sub>O absorption band near 6.4  $\mu\text{m}$  for a cloudy atmosphere. O<sub>2</sub>-X CIA strongly dominates the absorption in this wavelength range. The bottom panel shows how the strengths of O<sub>2</sub> monomer and CIA absorption features scale as a function of the O<sub>2</sub> atmospheric abundance for O<sub>2</sub> levels ranging from 0.1 times the present atmospheric level of O<sub>2</sub> (PAL) to 2 times PAL. Our results show that the 6.4  $\mu\text{m}$  CIA feature appears to be about three times stronger than the 1.27  $\mu\text{m}$  O<sub>2</sub> CIA feature and is therefore the strongest O<sub>2</sub> signature across the VIS/NIR/MIR spectrum.

Figure 2 shows the number of TRAPPIST-1e transits needed to detect the O<sub>2</sub> A-band, the O<sub>2</sub>-O<sub>2</sub> CIA feature at 1.27  $\mu\text{m}$  and the O<sub>2</sub>-X CIA feature at 6.4  $\mu\text{m}$  features at a 5  $\sigma$  confidence level with JWST for a modern Earth-like cloudy atmosphere on TRAPPIST-1e orbiting a TRAPPIST-1-like star at distances from Earth ranging from TRAPPIST-1’s true distance (12.1 pc) down to 2 pc. We can see that the 6.4  $\mu\text{m}$  O<sub>2</sub>-X CIA feature requires an order of magnitude fewer transits than the two other O<sub>2</sub> features because of the stronger intrinsic O<sub>2</sub>-X CIA absorption at 6.4  $\mu\text{m}$  and because cloud opacity is stronger at shorter VIS/NIR wavelengths. The horizontal dashed red line represents the 85 transits that will occur for TRAPPIST-1e during the 5.5 year nominal lifetime of JWST, thus sets up an upper limit on the number of transits observable. Because TRAPPIST-1e orbits a very small M8 star, it offers one of the best SNR a habitable planet can have and therefore represents a best-case scenario in terms of detectability. However, even in this context, none of the O<sub>2</sub> features are detectable at 5  $\sigma$  at the distance of the TRAPPIST-1 system. However, the 6.4  $\mu\text{m}$  O<sub>2</sub>-X CIA feature could be detectable at 5  $\sigma$  for an analogue system at star-Earth distance closer than 5 pc. Therefore, this simulation shows that the 6.4  $\mu\text{m}$  O<sub>2</sub>-X CIA could be the only oxygen feature detectable with JWST for a cloudy modern Earth-like atmosphere for nearby hypothetical TRAPPIST-1 analogue systems.

The O<sub>2</sub>-X feature for oxygen could also potentially be used to detect non-habitable conditions, such as a desiccated atmosphere rich in bars of abiotic O<sub>2</sub> generated from massive ocean loss (Wordsworth & Pierrehumbert, 2014; Luger & Barnes, 2015; Schwieterman et al., 2016; Meadows, 2017; Meadows et al., 2018; Lustig-Yaeger et al., 2019). Lincowski et al. (2018) have shown that for an assumed original water content of 20 Earth oceans (by mass), the TRAPPIST-1e, f and g planets may have lost between 3 to 6 Earth oceans resulting in atmospheres with 22 and 5,000 bars of O<sub>2</sub>.

Figure 3 shows transit spectra for TRAPPIST-1e assuming conservative 1 bar O<sub>2</sub>-only desiccated and isothermal atmospheres ranging from 200 to 600 K. Relative transit depth (ppm, left Y-axis) is the transit depth produced by the atmosphere itself, which can be converted into relative transit atmospheric thickness

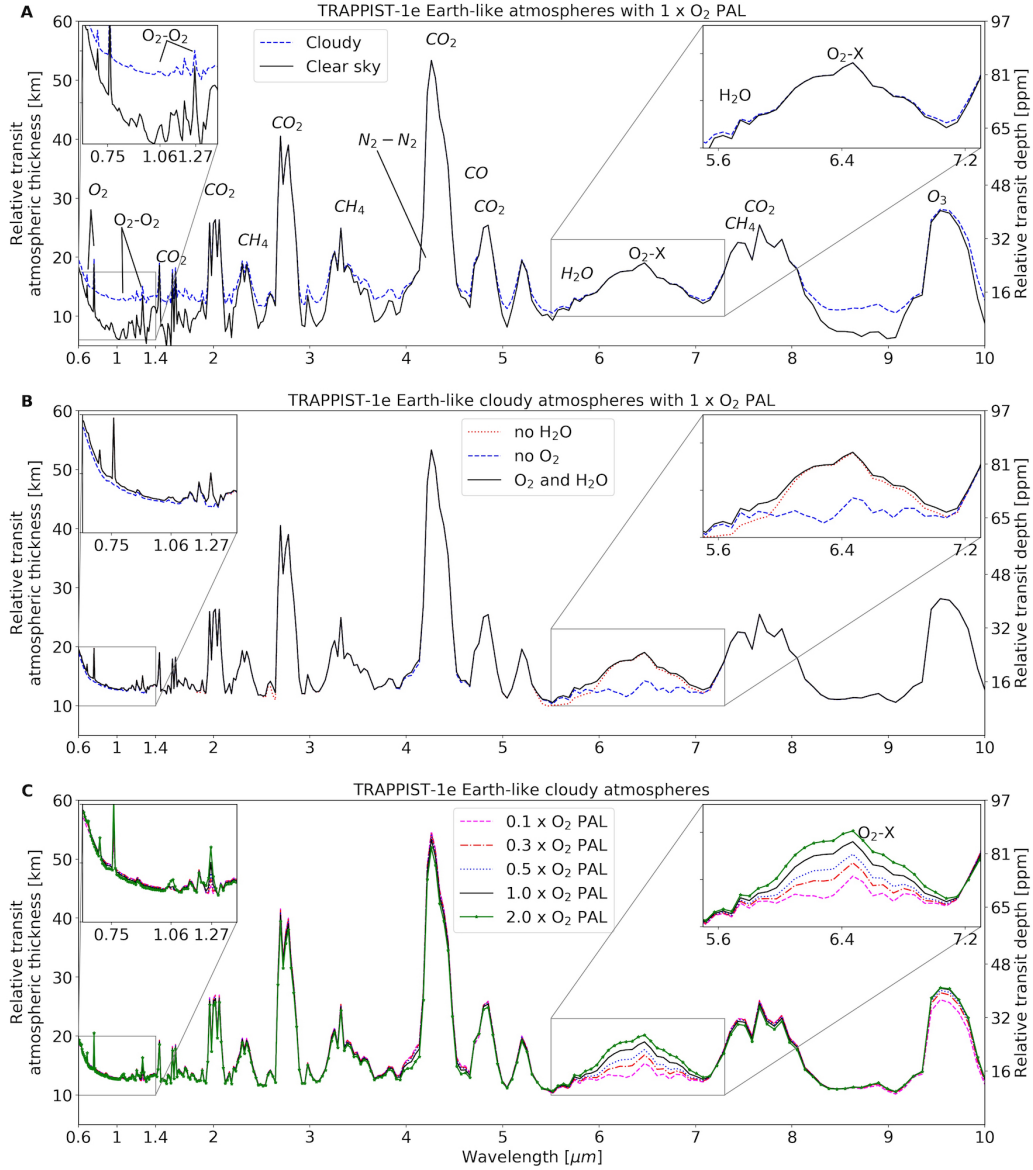


Figure 1: Shown are Earth-like transmission spectra of TRAPPIST-1e. Panel A: the impact of cloud coverage on the atmosphere’s spectral features. Panel B: a comparison of the strengths of the O<sub>2</sub>-X CIA feature and the H<sub>2</sub>O absorption band around 6.4  $\mu\text{m}$  for a cloudy atmosphere. Panel C: the strength of O<sub>2</sub> monomer absorptions and CIA features as a function of the amount of O<sub>2</sub> in the atmosphere relative to PAL for a spectrum with clouds included. The O<sub>2</sub>-X CIA could be the strongest O<sub>2</sub> feature across the VIS/NIR/MIR spectrum.

(km, right Y-axis). These isothermal profiles allow us to test the sensitivity of oxygen spectral features on atmospheric temperature. The atmospheric scale height increases with temperature, and the largest features are seen for the highest temperatures. Note that O<sub>2</sub>-O<sub>2</sub> CIA opacities in HITRAN are only provided in the 193 K–353 K temperature range. Therefore, for the isothermal profiles beyond 353 K we used the 353-K CIA coefficients. We can see that the 6.4  $\mu\text{m}$  O<sub>2</sub>-O<sub>2</sub> CIA feature is broad ( $\sim 3 \mu\text{m}$ ) and strong (40 to 90 ppm). The 1.27  $\mu\text{m}$  O<sub>2</sub>-O<sub>2</sub> CIA feature reaches a similar relative transit depth but is comparatively narrower (widths of  $\sim 0.2 \mu\text{m}$ ). In addition, the continuum level for the shorter wavelengths is raised by Rayleigh

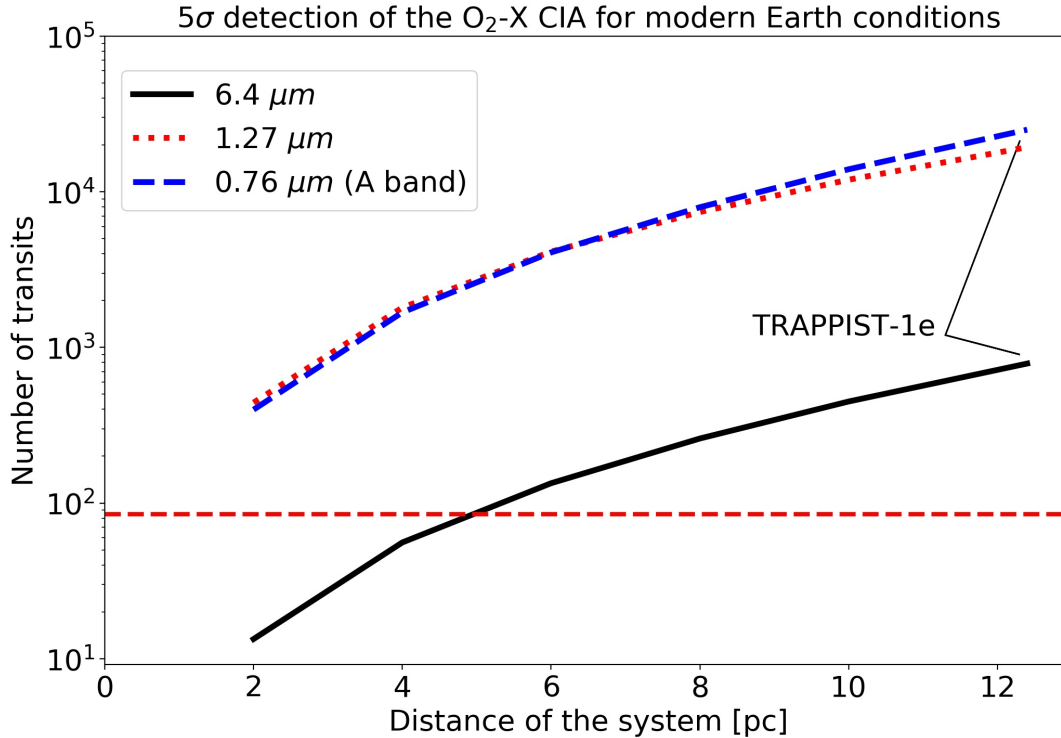


Figure 2: Number of TRAPPIST-1e transits needed for a  $5\sigma$  detection of the  $O_2$  A-band ( $R=100$ ), the  $O_2$ - $O_2$  CIA at  $1.27\ \mu m$  ( $R=100$ ) and the  $O_2$ -X CIA at  $6.4\ \mu m$  ( $R=30$ ) with JWST for the TRAPPIST-1 system moved from its distance to Sun (12.1 pc) down to 2 pc. The atmosphere is composed of  $N_2$ , 10,000 ppm of  $CO_2$ , 10 ppm of  $CH_4$ , 21% of  $O_2$  with a surface pressure of 1 bar. Resolving power ( $R$ ) has been optimized for each band to maximize the SNR. The horizontal dashed red line corresponds to the number of times TRAPPIST-1e will be observable transiting in front of TRAPPIST-1 during JWST 5.5 years life time (85 transits). The  $6.4\ \mu m$   $O_2$ -X CIA requires much less transits than the  $O_2$  A-band and the  $1.27\ \mu m$   $O_2$ - $O_2$  CIA and can be detectable at  $5\sigma$  for a TRAPPIST-1/TRAPPIST-1e analogue system closer than 5 pc.

scattering slope, reducing the NIR CIA relative transit depths to 50 to 80 ppm, respectively. Similarly, the  $O_2$  A-band reaches very high transit depths (up to 110 ppm) but on a high continuum, which reduces its relative strength down to 95 ppm. The larger width of the  $O_2$ -X CIA feature at  $6.4\ \mu m$  allows us to bin down the data to a lower resolving power, improving the SNR and therefore compensating for a higher noise floor in the MIRI LRS range. Supplementary Table 1 presents the relative transit depth, 1 transit SNR and number of transits for 3 and  $5\sigma$  detections for TRAPPIST-1e assuming 1 and 22 bar desiccated atmosphere on TRAPPIST-1e and Supplementary Figure 3 is similar to Fig. 2 but for the 22 bar  $O_2$  desiccated and isothermal atmospheres.

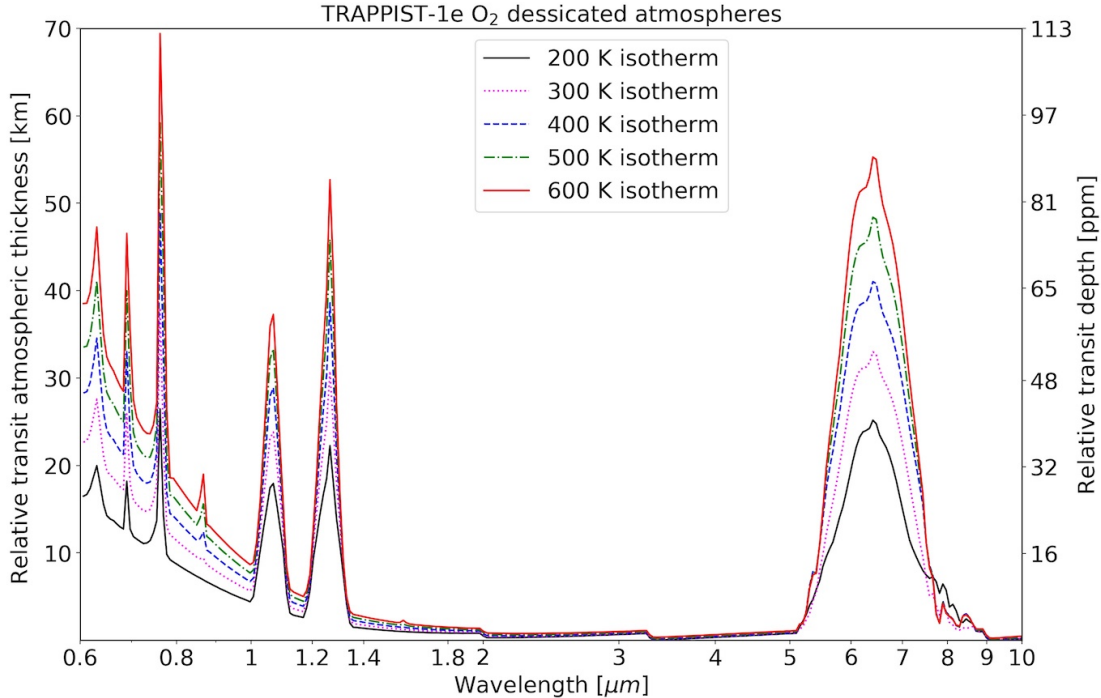


Figure 3: Transmission spectra for a 1 bar  $\text{O}_2$  desiccated atmosphere on TRAPPIST-1e assuming various isothermal profiles. Depending on the temperature, the  $6.4 \mu\text{m}$   $\text{O}_2$ - $\text{O}_2$  CIA feature can reach between 40 to 90 ppm, which is comparable or larger to the  $\text{O}_2$  A-band and  $1.06$  and  $1.27 \mu\text{m}$   $\text{O}_2$  CIA features. No photochemistry is considered here so  $\text{O}_3$  is missing in the spectra. Note that the increase of the relative transit atmospheric thickness and relative transit depth is due to the increase of the scale height with temperature.

Interpreting an  $\text{O}_2$  detection via the  $\text{O}_2$ - $\text{O}_2$  CIA band at  $6.4 \mu\text{m}$  will be strengthened by constraining the concentration of  $\text{O}_2$ , and placing its presence in a broader atmospheric context. For HZ planets with a planet/star contrast comparable to TRAPPIST-1e and within 5 pc from the Sun, next-generation MIR observatories could detect  $\text{O}_2$  in concentrations similar to modern Earth using the  $6.4 \mu\text{m}$   $\text{O}_2$ -X feature. In combination with detections of other MIR features from  $\text{CH}_4$ ,  $\text{H}_2\text{O}$ , or  $\text{N}_2\text{O}$ , this would represent a strong biosignature with no known non-biological explanations (Des Marais et al., 2002). Note that there are 50 red dwarfs within 5 pc from the Sun (<http://www.recons.org/TOP100.posted.htm>).

For systems farther than about 5 pc and/or HZ planet orbiting earlier M dwarfs, JWST or future MIR observatories may be able to detect the  $6.4 \mu\text{m}$   $\text{O}_2$ -X feature only for  $\text{O}_2$  concentrations orders of magnitude higher than those on modern-day Earth that would be indicative of a desiccated,  $\text{O}_2$ -rich, uninhabitable planet. Detection of this feature for planets within the habitable zone (Kasting et al., 1993; Kopparapu et al., 2013, 2014) will test the hypothesis that the high luminosity pre-main sequence phase M dwarfs endure can render even current HZ planets uninhabitable (Luger & Barnes, 2015). Finally, detection of this feature would answer the question of whether planets around M dwarfs can sustain an atmosphere.

## Methods

**Parameters for TRAPPIST-1e** In this study, TRAPPIST-1e planet’s parameters have been set up from (Gillon et al., 2017; Grimm et al., 2018). The TRAPPIST-1 spectrum of Lincowski et al. (2018) has been used for our photochemical simulations with the Atmos model.

**Monomer and CIA pressure sensitivity** Monomer and CIA optical depths can be expressed by the following equations (Misra et al., 2014):

$$d\tau_{mono} = \sigma\rho dl = \sigma P/Tdl \quad (1)$$

$$d\tau_{CIA} = k\rho^2 dl = k(P/T)^2 dl \quad (2)$$

with  $d\tau_{mono}$  and  $d\tau_{CIA}$  representing the monomer and CIA differential optical depths, respectively;  $\sigma$  and  $k$  are the monomer and CIA cross sections, respectively;  $\rho$  is the number density of the gas;  $P$  is the pressure;  $T$  is the temperature; and  $dl$  is the path length.  $d\tau_{mono}$  is proportional to  $P$  and  $d\tau_{CIA}$  to  $P^2$ , and this difference of sensitivity may be used to estimate the atmospheric pressure (Misra et al., 2014).

**The atmospheric modeling** We use the Atmos (Arney et al., 2016) photochemical model to self-consistently simulate Earth-like atmospheres with a variety of  $O_2$  partial pressures on TRAPPIST-1e. The terminator temperature, gas mixing ratio, vapor and condensed water (liquid and ice) profiles have been provided from the LMD-G (Wordsworth et al., 2011) global climate model (GCM) simulations of a 1 bar TRAPPIST-1e modern Earth atmosphere. In Atmos, some of the  $N_2$  has been swapped for  $O_2$  to obtain various  $O_2$  PAL as shown in Fig. 1, both gases having no greenhouse effect except through pressure broadening or CIA, and 10,000 ppm of  $CO_2$  and 10 ppm of  $CH_4$  have been assumed. Due to the terminator atmospheric profiles varying with latitude, Atmos was used to calculate profiles for 98 latitude points, determined by the LMD-G latitude resolution.

**Transmission spectra simulations** The planetary spectrum generator (PSG, Villanueva et al. (2018)) has been used to simulate JWST transmission spectra. PSG is an online radiative-transfer code that is able to compute planetary spectra (atmospheres and surfaces) for a wide range of wavelengths (UV/Vis/near-IR/IR/far-IR/THz/sub-mm/Radio) from any observatory, orbiter or lander and also includes a noise calculator. To compute the noise, PSG takes into account the noise introduced by the source itself ( $N_{source}$ ), the background noise ( $N_{back}$ ) following a Poisson distribution with fluctuations depending on  $\sqrt{N}$  with  $N$  the mean number of photons received (Zmuidzinas, 2003), the noise of the detector ( $N_D$ ) and the noise introduced by the telescope ( $N_{optics}$ ). The total noise being then  $N_{total} = \sqrt{N_{source} + N_{back} + N_D + N_{optics}}$ . This represents therefore a photon limited situation where  $N_{source}$  will largely dominate  $N_{total}$ . For the Earth-like atmospheres, spectra were obtained for each of the 98 Atmos photochemical simulations and an average spectrum was computed. For the 1 and 22 bar  $O_2$  desiccated atmospheres, isothermal profiles from 200 to 600 K were set up with 100% of  $O_2$ , ignoring photochemistry. To calculate the SNR and the number of transits needed for 3 and 5 $\sigma$  detection the resolving power has been optimized by adjusting the binning for each  $O_2$  feature to maximize its SNR. SNR is calculated using the highest value in the band minus the nearest continuum value (this value therefore differ between the VIS (Rayleigh slope), NIR and MIR). The number of transits needed to achieve a  $X\sigma$  detection is computed as the following equation:

$$N_{transits}^{X\sigma} = N_i * (X/SNR_i)^2 \quad (3)$$

with  $X\sigma$  the confident level of value  $X$ ,  $N_i$  is the initial number of transit at which  $SNR_i$  is computed. If  $SNR_i$  is estimated from 1 transit then  $N_i = 1$  and the Eq. 3 could be simplified as:

$$N_{transits}^{X\sigma} = (X/SNR_i)^2 \quad (4)$$

**$O_2$ -X collision-induced absorption at 6.4  $\mu m$ .** This feature is associated with the fundamental band of  $O_2$ , and  $O_2$  collisions with other partners (e.g.  $N_2$ ,  $CO_2$ ) can produce additional absorption at these wavelengths. This collision with other gases can be generally written as  $O_2$ -X, where "X" refers to the collision partner. Laboratory measurements (Timofeyev & Tonkov, 1978; Thibault et al., 1997) and atmospheric analysis using Sun occultations (Rinsland et al., 1989) have revealed that nitrogen, the major constituent of modern Earth's atmosphere at 78% in volume, produces an  $O_2$ - $N_2$  absorption feature of a similar intensity as  $O_2$ - $O_2$  in the 6.4  $\mu m$  region. Carbon dioxide ( $CO_2$ ) can also produce an  $O_2$ - $CO_2$  feature at these wavelengths, though this feature is weak for modern Earth-like  $CO_2$  atmospheric abundances (approx. 400 ppm) but can be strong for exoplanets with  $CO_2$  rich atmospheres (Baranov et al., 2004).  $O_2$ -X CIA can also be

produced with H<sub>2</sub>O (Hopfner et al., 2012) as the collision partner due to the large electric dipole moment of H<sub>2</sub>O, but no laboratory measurements exist for this feature.

**Parameterization of the 6.4  $\mu\text{m}$  feature** While the 6.4  $\mu\text{m}$  region is known as the fundamental vibration-rotation band of O<sub>2</sub>, only the O<sub>2</sub>-O<sub>2</sub> CIA band is included in HITRAN (Gordon et al., 2017). Knowing that Earth's atmosphere is mostly composed of N<sub>2</sub> and that the O<sub>2</sub>-N<sub>2</sub> CIA have been shown to produce similar absorption to O<sub>2</sub>-O<sub>2</sub> (Timofeyev & Tonkov, 1978; Rinsland et al., 1989; Thibault et al., 1997), it is important to include it in our simulations. We have parameterized the O<sub>2</sub>-N<sub>2</sub> CIA in PSG assuming the same absorption efficiency as O<sub>2</sub>-O<sub>2</sub> CIA (Rinsland et al., 1989) (see Supplementary Figure 1). For O<sub>2</sub>-CO<sub>2</sub> CIA at 6.4  $\mu\text{m}$ , we used experimental data of Baranov et al. (2004) to include that feature in PSG.

## References

- Arney, G., Domagal-Goldman, S. D., Meadows, V. S., et al. 2016, *Astrobiology*, 16, 873
- Baranov, Y. I., Lafferty, W., & Fraser, G. 2004, *J MOL SPECTROSC*, 228, 432 , special Issue Dedicated to Dr. Jon T. Hougen on the Occasion of His 68th Birthday. <http://www.sciencedirect.com/science/article/pii/S0022285204001390>
- Des Marais, D. J., Harwit, M. O., Jucks, K. W., et al. 2002, *Astrobiology*, 2, 153
- Faucher, T., Rossi, L., & Stam, D. M. 2017, *ASTROPHYS J*, 842, 41
- Gillon, M., Triaud, A. H. M. J., Demory, B.-O., et al. 2017, *Nature*, 542, 456–460. <https://doi.org/10.1038/nature21360>
- Gordon, I., Rothman, L., Hill, C., et al. 2017, *J QUANT SPECTROSC RA*, 203, 3 , hITRAN2016 Special Issue. <http://www.sciencedirect.com/science/article/pii/S0022407317301073>
- Grimm, S. L., Demory, B.-O., Gillon, M., et al. 2018, *ASTRON ASTROPHYS*, 613, A68
- Hopfner, M., Milz, M., Buehler, S., Orphal, J., & Stiller, G. 2012, *GEOPHYS RES LETT*, 39, <https://agupubs.onlinelibrary.wiley.com/doi/pdf/10.1029/2012GL051409>
- Kasting, J. F., Whitmire, D. P., & Reynolds, R. T. 1993, *Icarus*, 101, 108 . <http://www.sciencedirect.com/science/article/pii/S0019103583710109>
- Kopparapu, R. K., Ramirez, R. M., SchottelKotte, J., et al. 2014, *ASTROPHYS J*, 787, L29. <https://doi.org/10.1088%2F2041-8205%2F787%2F2%2F129>
- Kopparapu, R. K., Ramirez, R., Kasting, J. F., et al. 2013, *ASTROPHYS J*, 765, 131. <http://stacks.iop.org/0004-637X/765/i=2/a=131>
- Lincowski, A. P., Meadows, V. S., Crisp, D., et al. 2018, *ASTROPHYS J*, 867, 76
- Luger, R., & Barnes, R. 2015, *Astrobiology*, 15, 119
- Lustig-Yaeger, J., Meadows, V. S., & Lincowski, A. P. 2019, *ASTRON J*, 158, 27. <https://doi.org/10.3847%2F1538-3881%2Fab21e0>
- Meadows, V. S. 2017, *Astrobiology*, 17, 1022, PMID: 28443722. <https://doi.org/10.1089/ast.2016.1578>
- Meadows, V. S., Reinhard, C. T., Arney, G. N., et al. 2018, *Astrobiology*, 18, 630, PMID: 29746149. <https://doi.org/10.1089/ast.2017.1727>
- Misra, A., Meadows, V., Claire, M., & Crisp, D. 2014, *Astrobiology*, 14, 67

- Pallé, E., Zapatero Osorio, M. R., Barrena, R., Montañés-Rodríguez, P., & Martín, E. L. 2009, *Nature*, 459, 814
- Rinsland, C. P., Smith, M. A. H., Seals Jr., R. K., et al. 1982, *J GEOPHYS RES-OCEANS*, 87, 3119
- Rinsland, C. P., Zander, R., Namkung, J. S., Farmer, C. B., & Norton, R. H. 1989, *J GEOPHYS RES-ATMOS*, 94, 16303
- Schwieterman, E. W., Meadows, V. S., Domagal-Goldman, S. D., et al. 2016, *ASTROPHYS J*, 819, L13
- Snellen, I. A. G., de Kok, R. J., le Poole, R., Brogi, M., & Birkby, J. 2013, *ASTROPHYS J*, 764, 182. <https://doi.org/10.1088%2F0004-637x%2F764%2F2%2F182>
- Thibault, F., Menoux, V., Doucen, R. L., et al. 1997, *APPL OPTIC*, 36, 563. <http://ao.osa.org/abstract.cfm?URI=ao-36-3-563>
- Timofeyev, Y., & Tonkov, M. 1978, *Izv. Acad. Sci. USSR Atmos. Ocean. Phys.*, Engl. Transl., 14, 614
- Villanueva, G. L., Smith, M. D., Protopapa, S., Faggi, S., & Mandell, A. M. 2018, *J QUANT SPECTROSC RA*, 217, 86
- Wordsworth, R., & Pierrehumbert, R. 2014, *ASTROPHYS J*, 785, L20
- Wordsworth, R. D., Forget, F., Selsis, F., et al. 2011, *ASTROPHYS J LETT*, 733, L48
- Zmuidzinas, J. 2003, *APPL OPTIC*, 42, 4989. <http://ao.osa.org/abstract.cfm?URI=ao-42-25-4989>

**Data availability** The data that support the plots within this paper and other findings of this study are available from the corresponding author upon reasonable request.

**Code availability** Atmos (Arney et al., 2016) is available upon request from Giada Arney ([giada.n.arney@nasa.gov](mailto:giada.n.arney@nasa.gov)); LMD-G (Wordsworth et al., 2011) is available upon request from Martin Turbet ([martin.turbet@lmd.jussieu.fr](mailto:martin.turbet@lmd.jussieu.fr)); PSG (Villanueva et al., 2018) is available on <https://psg.gsfc.nasa.gov/>.

**Acknowledgements** T. Fauchez, G. Villanueva, G. Arney, R. Kopparapu, A. Mandell and S. Domagal-Goldman acknowledge support from GSFC Sellers Exoplanet Environments Collaboration (SEEC), which is funded in part by the NASA Planetary Science Divisions Internal Scientist Funding Model.

This project has received funding from the European Union's Horizon 2020 research and innovation program under the Marie Skłodowska-Curie Grant Agreement No. 832738/ESCAPE.

This work was also supported by the NASA Astrobiology Institute Alternative Earths team under Cooperative Agreement Number NNA15BB03A and the NExSS Virtual Planetary Laboratory under NASA grant number 80NSSC18K0829. E.W.S. is additionally grateful for support from the NASA Postdoctoral Program, administered by the Universities Space Research Association. We thank Ha Tran for useful discussions related to O<sub>2</sub>-X CIAs. Finally, we would like to thank the two anonymous referees for comments that greatly improved our manuscript.

**Author contributions** T.J.F. led the photochemistry and transmission spectroscopy simulations. G.L.V, E.W.S and M.T. derived parameterizations of the O<sub>2</sub>-N<sub>2</sub> and O<sub>2</sub>-CO<sub>2</sub> CIAs bands. T.J.F and G.A. wrote most of the manuscript. Every author contributed to the discussions and to the writing of the manuscript.

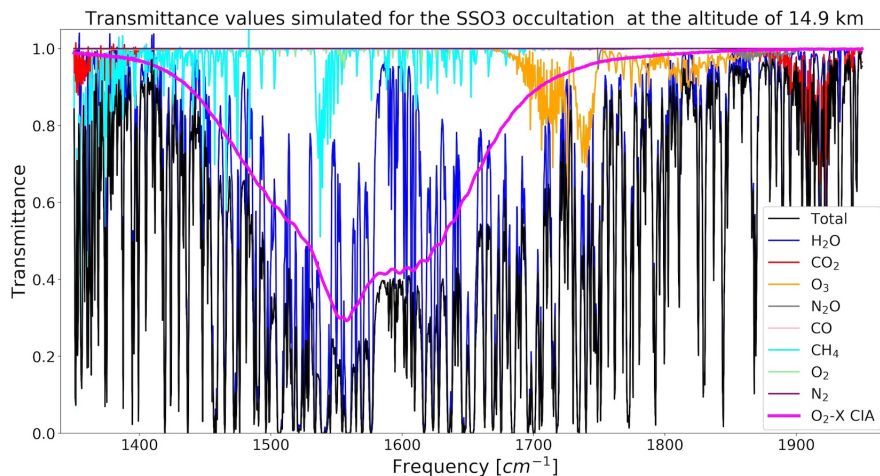
**Reviewer information** The authors declare no competing financial interests. Readers are welcome to comment on the online version of the paper.

**Competing interest** The authors declare no competing financial interests.



## Supplementary materials

**Overview of previous works on O<sub>2</sub> spectral features for exoplanet’s studies.** Because O<sub>2</sub> is one of the most detectable and robust indicators of global biological activity, concepts for telescopes that would attempt to search for life on exoplanets all include the ability to detect O<sub>2</sub> or its photochemical byproduct, O<sub>3</sub>. O<sub>2</sub> absorbs at several wavelengths in the visible (VIS) at 0.63, 0.69 and 0.76  $\mu\text{m}$  and near-infrared (NIR) at 1.27  $\mu\text{m}$ . The O<sub>2</sub> A-band at 0.76  $\mu\text{m}$  has often been considered the most viable spectral feature for oxygen detection in transmission (Snellen et al., 2013) and reflectance spectra (Fauchez et al., 2017). Snellen et al. (2013) showed that it could be possible to detect the O<sub>2</sub> A-band in the atmosphere of an Earth twin with the future Extremely Large Telescopes (ELTs). However large unknowns remain to disentangle the exoplanet O<sub>2</sub> signal from the telluric O<sub>2</sub>. Meanwhile, Pallé et al. (2009) showed that O<sub>2</sub>-O<sub>2</sub> collision induced absorption (CIA) features at 1.06 and 1.27  $\mu\text{m}$  were present in Earth’s transmission spectrum during lunar eclipse and produce more absorption than the O<sub>2</sub> A-band monomer feature. CIA features are produced through inelastic collisions in a gas. In the case of the O<sub>2</sub>-O<sub>2</sub> CIA features, the two O<sub>2</sub> molecules interact forming transient multipole-induced dipoles producing broad spectral features distinct from the individual underlying O<sub>2</sub> molecule. Misra et al. (2014) showed that the 1.06 and 1.27  $\mu\text{m}$  O<sub>2</sub>-O<sub>2</sub> CIA features may be detectable (for SNR > 3) with the James Webb Space Telescope (JWST) for an Earth analogue orbiting an M5V star at a distance of 5 pc. Schwieterman et al. (2016) proposed that the 1.06 and 1.27  $\mu\text{m}$  transit features could be used to identify the high O<sub>2</sub> partial pressures predicted to be associated with abiotic O<sub>2</sub> atmospheres, which should be significantly higher than for the modern Earth case. More recently, Lustig-Yaeger et al. (2019) have shown that the 1.06 and 1.27  $\mu\text{m}$  O<sub>2</sub> CIA features could be detectable with JWST at a SNR of 5 in just few transits for the TRAPPIST-1 planets with O<sub>2</sub> desiccated and dense (10 and 100 bars) atmospheres.

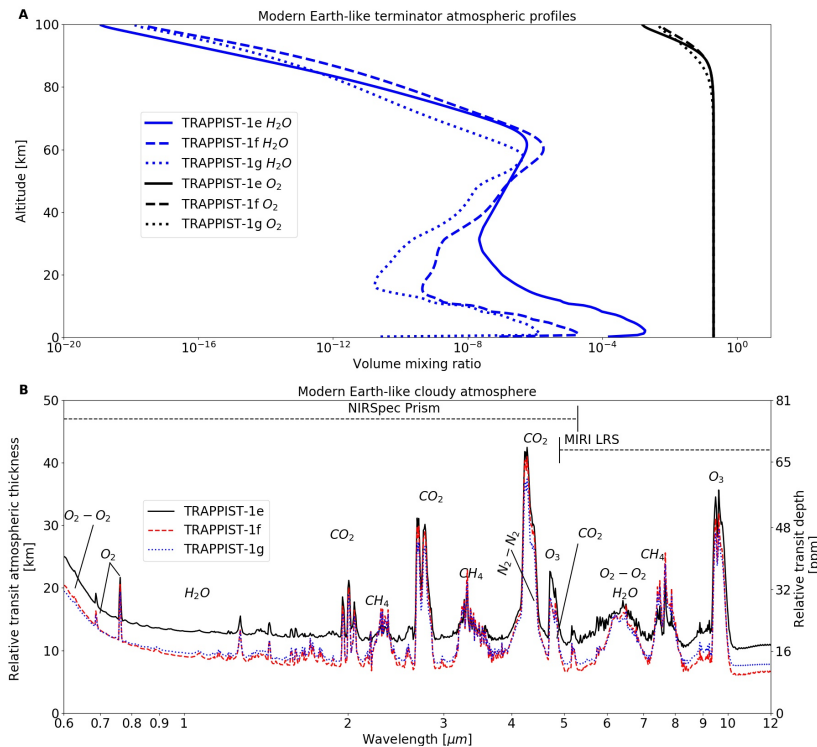


Supplementary Figure 1: Simulation with PSG of the SSO3 occultation observed by Rinsland et al. (1989) April 30, 1985 at an altitude of 14.9 km over the latitude 32.3°N and longitude 290.6°W. Simulation of the 6.4  $\mu\text{m}$  O<sub>2</sub>-X CIA is in very good agreement with observation data from (Rinsland et al., 1989).

Supplementary Figure 1 shows the simulation of the Sun occultation SSO3 observed by Rinsland et al. (1989) (figure 3) on April 30, 1985, at an altitude of 14.9 km (13 km over the Himalayas). Our simulation and the observation data are in very good agreement, showing the validity of our O<sub>2</sub>-X CIA parameterization at 6.4  $\mu\text{m}$ .

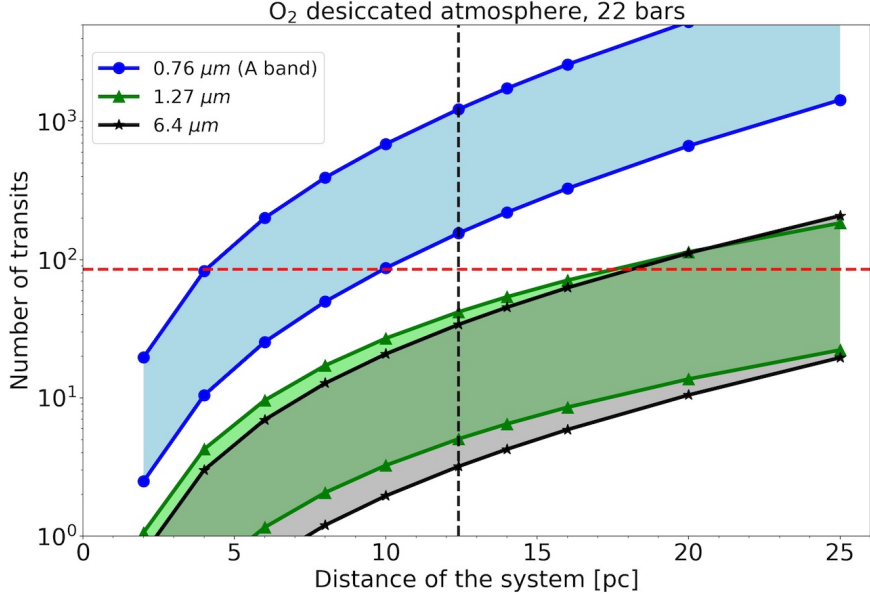
Supplementary Figure 2 shows the terminator H<sub>2</sub>O and O<sub>2</sub> atmospheric profiles with a modern Earth-like atmosphere composition for TRAPPIST-1 planets in the habitable zone, namely 1e, 1f and 1g (top panel) and their transmission spectrum with clouds included (bottom panel). Boundary conditions for the photochemistry are those described in Lincowski et al. (2018) Table 8. We can see that the terminator region is very dry, with volume mixing ratios near the surface reaching the maximum value 10<sup>-3</sup> for TRAPPIST-1e

decreasing down to  $10^{-6}$  for 1g. However, as we can see in the spectra this region of maximum  $\text{H}_2\text{O}$  concentration is below the continuum level because of clouds and atmospheric refraction. Note that above  $\sim 60$  km  $\text{H}_2\text{O}$  is strongly photodissociated. As a results, the contribution of  $\text{H}_2\text{O}$  at  $6.4 \mu\text{m}$  is very largely dominated by the  $\text{O}_2\text{-X}$  CIA and this domination increase for dryer planets TRAPPIST-1f and 1g.



Supplementary Figure 2: Panel A:  $\text{H}_2\text{O}$  and  $\text{O}_2$  atmospheric profiles at the terminator of TRAPPIST-1e, 1f and 1g planets in the habitable zone with a modern Earth-like atmosphere. Panel B: Corresponding transmission spectra for the three planets. We can see that  $\text{H}_2\text{O}$  volume mixing ratio is tiny by comparison to  $\text{O}_2$  and that the wetter region near the surface is below the continuum level of the spectra because of the atmospheric refraction and/or clouds.  $\text{O}_2\text{-X}$  largely dominates over  $\text{H}_2\text{O}$  in the  $6.4 \mu\text{m}$  region.

Supplementary Figure 3 is similar to Fig. 2 but for the 22 bar  $\text{O}_2$  desiccated and isothermal atmospheres presented in Table 1. We can see that the  $\text{O}_2\text{-O}_2$   $1.27 \mu\text{m}$  CIA and  $\text{O}_2\text{-X}$   $6.4 \mu\text{m}$  CIA features require significantly fewer transits than the  $\text{O}_2$  A-band monomer band and would be detectable at up to about 25 pc (except for the coldest isothermal atmosphere beyond 20 pc). Note that in the case of a desiccated,  $\text{O}_2$ -rich planet with aerosols, the  $6.4 \mu\text{m}$  band would require significantly fewer transits than the  $1.27 \mu\text{m}$  for the same reasons as for the habitable case.



Supplementary Figure 3: Number of TRAPPIST-1e transits needed for a  $5\sigma$  detection of the  $\text{O}_2$  A-band ( $R=100$ ), the  $\text{O}_2\text{-O}_2$  CIA at  $1.27\ \mu\text{m}$  ( $R=20$ ) and the  $\text{O}_2\text{-X}$  CIA at  $6.4\ \mu\text{m}$  ( $R=10$ ) with JWST for the TRAPPIST-1 system moved from 2 to 25 pc away from the Sun. The atmosphere is exclusively composed of  $\text{O}_2$  with surface pressure of 22 bars. For each wavelength the shaded area correspond to various isothermal profiles from 600 K (lowest line) to 200 K (highest line). Resolving power ( $R$ ) has been optimized for each band to maximize the SNR. The horizontal dashed red line corresponds to the number of times TRAPPIST-1e will transits during JWST 5.5 years life time (85 transits). The vertical dashed black line denotes the distance of the TRAPPIST-1 system with respect to the Sun. The  $\text{O}_2\text{-O}_2$  CIA at  $1.27\ \mu\text{m}$  and the  $\text{O}_2\text{-X}$  CIA at  $6.4\ \mu\text{m}$  are detectable up to 25 pc away, except for the coldest atmospheres beyond 20 pc.

Supplementary Table 1 presents the relative transit depth, 1 transit SNR and number of transits for 3 and  $5\sigma$  detections for TRAPPIST-1e assuming 1 and 22 bar desiccated atmosphere on TRAPPIST-1e. 22 bars is based on a conservative estimate of  $\text{O}_2$  retention by Lincowski et al. (2018). We can see that the difference in transit depth between the 1 and 22 bar cases increase with temperature (because the refraction limit is at higher pressures) and that the strength of  $\text{O}_2$  A-band is relatively insensitive to pressure. The  $\text{O}_2\text{-X}$  CIA feature at  $6.4\ \mu\text{m}$  requires fewer transits to achieve 3 or  $5\sigma$  detection and is therefore the most promising indicator of a massive  $\text{O}_2$  desiccated atmosphere potentially observable with JWST.

Supplementary Table 1: Relative transit depth (ppm), signal-to-noise ratio for 1 transit (SNR-1) and number of transits to achieve a  $5\sigma$  and  $3\sigma$  detection of  $O_2$  assuming  $O_2$  desiccated and isothermal atmospheres on TRAPPIST-1e Lincowski et al. (2018). The numbers at the left of the “-” mark are for the 1 bar atmosphere while the numbers at the right are for the 22 bar atmosphere. (-) represent the cases for which more than 100 integrated transits are needed. For each feature, the wavelength and resolving power (R) are mentioned.

Feature	A-band	$O_2$ - $O_2$	$O_2$ - $O_2$	$O_2$ -X
Wavelength [ $\mu m$ ]	0.76	1.06	1.27	6.4
R	100	40	20	10
Temperature	200 K			
Depth [ppm]	44-44	38-37	42-41	67-66
SNR-1	0.25-0.25	0.66-0.65	1.16-1.14	1.33-1.31
N transits ( $5\sigma$ )	(-)	57-59	19-19	14-15
N transits ( $3\sigma$ )	(-)	21-21	7-7	5-5
Temperature	300 K			
Depth [ppm]	68-68	52-62	57-71	88-107
SNR-1	0.39-0.39	0.90-1.07	1.59-1.98	1.75-2.13
N transits ( $5\sigma$ )	(-)	31-22	10-7	8-6
N transits ( $3\sigma$ )	59-59	11-8	4-3	3-2
Temperature	400 K			
Depth [ppm]	91-99	63-88	71-107	110-162
SNR-1	0.52-0.57	1.10-1.54	1.97-2.97	2.18-3.22
N transits ( $5\sigma$ )	93-77	21-11	6-3	5-2
N transits ( $3\sigma$ )	33-28	7-4	2-1	2-1
Temperature	500 K			
Depth [ppm]	114-127	74-108	83-132	129-197
SNR-1	0.65-0.73	1.28-1.88	2.31-3.65	2.56-3.91
N transits ( $5\sigma$ )	59-47	15-7	5-2	4-2
N transits ( $3\sigma$ )	21-17	6-3	2-1	1-1
Temperature	600 K			
Depth [ppm]	137-156	83-136	95-174	147-264
SNR-1	0.79-0.89	1.44-2.37	2.63-4.83	2.93-5.23
N transits ( $5\sigma$ )	40-32	12-5	4-1	3-1
N transits ( $3\sigma$ )	14-12	4-2	1	1-1

## References

- Faucher, T., Rossi, L., & Stam, D. M. 2017, *ASTROPHYS J*, 842, 41
- Lincowski, A. P., Meadows, V. S., Crisp, D., et al. 2018, *ASTROPHYS J*, 867, 76
- Lustig-Yaeger, J., Meadows, V. S., & Lincowski, A. P. 2019, *ASTRON J*, **158**, 27. <https://doi.org/10.3847/2F1538-3881%2F20190101>
- Misra, A., Meadows, V., Claire, M., & Crisp, D. 2014, *Astrobiology*, 14, 67
- Pallé, E., Zapatero Osorio, M. R., Barrena, R., Montañés-Rodríguez, P., & Martín, E. L. 2009, *Nature*, 459, 814
- Rinsland, C. P., Zander, R., Namkung, J. S., Farmer, C. B., & Norton, R. H. 1989, *J GEOPHYS RES-ATMOS*, 94, 16303
- Schwietzman, E. W., Meadows, V. S., Domagal-Goldman, S. D., et al. 2016, *ASTROPHYS J*, 819, L13
- Snellen, I. A. G., de Kok, R. J., le Poole, R., Brogi, M., & Birkby, J. 2013, *ASTROPHYS J*, 764, 182. <https://doi.org/10.1088/2F0004-637x/2F764/2F2%2F182>